

IMECE2008-68823

A HEAT PLATE LEADING EDGE FOR HYPERSONIC VEHICLES

Scott D. Kasen
 University of Virginia
 Charlottesville, Va, USA

Doug T. Queheillalt
 University of Virginia
 Charlottesville, Va, USA

Craig A. Steeves
 University of California – Santa Barbara
 Santa Barbara, Ca, USA

Anthony G. Evans
 University of California – Santa Barbara
 Santa Barbara, Ca, USA

Haydn N. G. Wadley
 University of Virginia
 Charlottesville, Va, USA

ABSTRACT

The intense thermal flux at the leading edges of hypersonic vehicles (traveling at Mach 5 and greater) requires creative thermal management strategies to prevent damage to leading edge components. Carbon fiber composites and/or ablative coatings have been widely utilized to mitigate the effects of the impinging heat flux. This paper focuses on an alternative, metallic leading edge heat pipe concept which combines efficient structural load support and thermal management. The passive concept is based on high thermal conductance heat pipes which redistribute the high heat flux at the leading edge stagnation point through the evaporation, vapor flow, and condensation of a working fluid to a location far from the heat source. Structural efficiency is provided by a sandwich construction using an open-cell core that also allows for vapor flow.

A low temperature proof-of-concept copper–water system has been investigated by experimentation. Measuring of the axial temperature profile indicates effective spreading of thermal energy, a lowering of the maximum temperature and reduced overall thermal gradient compared to a non-heat pipe leading edge. A simple transient analytical model based on lumped thermal capacitance theory is compared with the experimental results. The low-temperature prototype shows potential for higher temperature metallic leading edges that can withstand the hypersonic thermo-mechanical environment.

INTRODUCTION AND BACKGROUND

During hypersonic flight, vehicle leading edges are subjected to intense localized heat fluxes. For vehicles under

hydrocarbon-fueled airbreathing propulsion, the aerodynamic requirements dictate the use of a sharp leading edge with a radius on the order of several millimeters. This presents a particularly challenging design issue, as it has been shown that the heat flux impinging upon a vehicles leading edge is inversely proportional to the square root of the leading edge radius (Fay and Riddell, 1958). The cold wall heat flux at the stagnation point can be approximated by;

$$q_{cw,st} \approx H_{\infty} K \sqrt{\frac{P_{st}}{R_{le}}} \quad (1)$$

where H_{∞} is the local fluid enthalpy at a given Mach number, K is a heat transfer factor of the fluid (for air, $K = 3.6 \times 10^{-4} \text{ m}^{-1} \text{ kg}^{-1/2}$), P_{st} is the pressure at the stagnation point, and R_{le} is the leading edge radius (Steeves *et al.*, 2008). Following the method of Steeves *et al.* (2008), Table 1 shows several calculated values of H_{∞} and P_{st} for Mach 6-8 flight at a dynamic pressure of 48kPa.

Mach No.	Altitude, (km)	Local Enthalpy, H_{∞} (MJ/kg)	Stagnation Pressure, P_{st} (kPa)
6	26.93	1.85	95.90
7	28.98	2.46	95.72
8	30.76	3.16	93.70

Table 1. Calculated stagnation conditions for Mach 6-8 flight at a dynamic pressure of 48kPa. Adapted from (Steeves *et al.*, 2008)

Using the values from Table 1, the estimated cold wall heat flux for several leading edge radii and flight velocities can be calculated, Figure 1. At the radii of interest for moderate hypersonic flight (1-5mm), the incident fluxes are on the order 1-10MW/m².

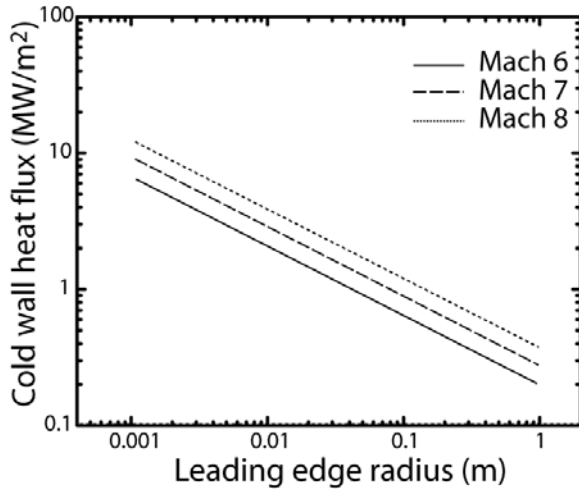


Figure 1. Calculated cold wall heat flux for several leading edge radii at Mach 6-8 and a dynamic pressure of 48kPa.

At such high heat fluxes, very high temperatures and large thermal gradients can be generated at the leading edge tip such that the thermal loads and imposed stress exceed the limits of many materials. The need for a thermal protection system (TPS) has stimulated interest in oxide coatings, high temperature composites, and ablative coatings (Kourtidis, 1993, Lundell, 1983, Paul *et al.*, 2000, Savino *et al.*, 2008).

Here, we consider an all-metallic, structurally efficient leading edge concept which relies on high conductance heat pipes to spread heat to regions far from the stagnation point for efficient removal by convection and/or radiation. The evaporation, vapor flow (thermal transport) and condensation of a working fluid far from the heat source isothermizes the structure, thereby lowering maximum temperatures and overall thermal gradients. An open-cell prismatic or truss core (Wadley, 2006) provides structural support to the leading edge and configures a pathway for easy vapor flow. In contrast to most TPS systems, the heat plate concept allows ingress of the heat flux to the airframe itself for redistribution and ejection.

This article is organized as follows. First, the heat plate concept is described, and an overview of its fundamental operation provided. Consideration is given to the choice of core topology that provides multifunctionality. Preliminary experimental work on a low-temperature copper-water system is presented, and a simple lumped thermal capacitance model is developed which predicts thermal behavior.

LEADING EDGE HEAT PLATE CONCEPT

Heat plate structure. Figure 2 is a schematic showing the leading edge concept. It comprises metallic face sheets which serve as the outer skin for radiating the displaced heat away from the structure and as the containment case for the fluid. Structural support is provided by a truncated honeycomb (cruciform) core which supports transverse and shear loads while permitting multidirectional (axial and transverse) vapor flow. The cruciforms and interior surfaces of the metallic face sheets are lined with a porous wick material for fluidic communication between the upper and lower face sheets and return of condensed fluid to the leading edge tip. The choice of core topology is not limited to the honeycomb structure shown in the figure. The mechanical and thermal properties of various topologies have been discussed elsewhere (Evans *et al.*, 1998, Evans *et al.*, 2001, Lim and Kang, 2006, Queheillalt and Wadley, 2005, Wadley, 2006, Wadley *et al.* 2003, Wei *et al.*, 2007, Wicks and Hutchinson, 2001). The choice of core topology and its predicted influence on the heat transfer rate is addressed later.

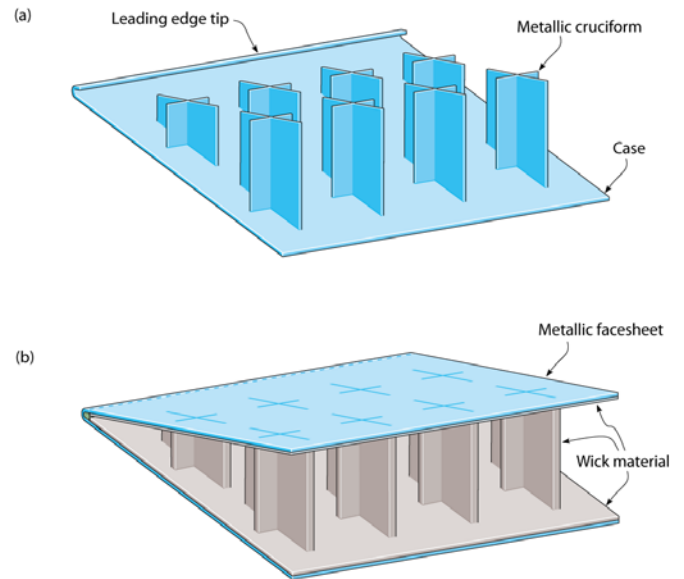


Figure 2. A heat plate having a truncated honeycomb core with (a) the wick and upper face sheet removed for clarity, and (b) both face sheets and wick installed. No side or rear face sheets are shown. From Steeves *et al.*, 2008.

Fundamental operation. Figure 3 illustrates the operating mechanism of the heat plate. Heat impinges the tip of the leading edge near the stagnation region and is thermally conducted through the face sheet to the saturated wick-vapor interface. Evaporation ensues which sets up a pressure gradient along the axial length (axis of cooling). The vapor carries the heat of vaporization down the pressure gradient where it condenses releasing its latent heat, thereby isothermizing the structure. The heat is transferred through the face sheet by thermal conduction, where it is removed from the surface by radiation or convection. The liquid is returned to the leading edge tip through the wick under molecular (adhesive and cohesive) forces. The magnitude of the

stagnation point heat flux at hypersonic velocities requires the use of a working fluid that combines a high latent heat of vaporization, surface tension, and high thermal conductivity at the temperature range of interest. Molten alkali metals have been proposed as a working fluid to meet these demands (Steeves *et al.*, 2008, Faghri, 1995).

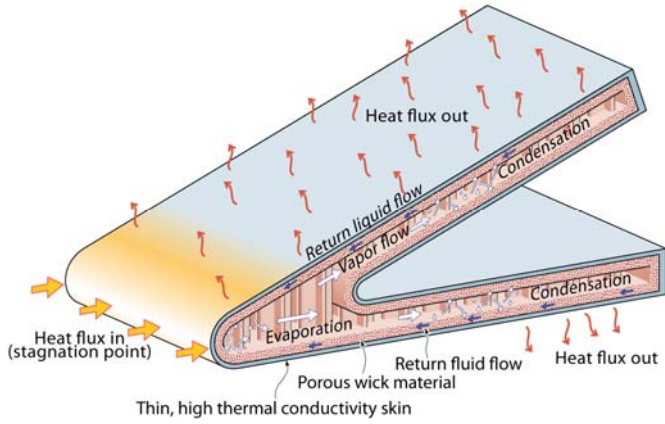


Figure 3. Fundamental operating phenomena of the leading edge heat plate. Thermal transport occurs via evaporation and vapor flow through the void created by the core (in this case, the cruciform members). The fluid condenses in the cooler areas where the heat is eventually released to the ambient. The liquid circulates back to the stagnation region through the wick.

Design considerations. As noted elsewhere (Chi, 1976), there are a number of heat transport limits that place an upper bound on the ultimate heat transfer of a heat plate at a given (isothermal) operating temperature. The limits most relevant to high temperature, liquid metal heat pipes are: *i*) the sonic limit, caused by a choking phenomenon normally occurring during startup when the heat pipe is operating with low vapor densities and high vapor velocities, *ii*) the capillary limit, which occurs when the summation of vapor and liquid pressure drops is equal to the available pumping pressure of the wick, and *iii*) the boiling limit, which occurs when bubbles nucleate in the evaporator zone, hindering the fluid return flow. Both the capillary and boiling limits result in evaporator dryout (Chi, 1976).

The capillary limit is reached when the sum of the liquid and pressure drops ($\Delta P_l + \Delta P_v$) equals the capillary pumping pressure of the wick (ΔP_c);

$$\Delta P_c = \Delta P_l + \Delta P_v \quad (2)$$

Under this condition, dryout ensues since the wick pumping pressure can no longer overcome the liquid pressure drop (from the flow of liquid through the often tortuous path of the wick) and vapor pressure drop. Earlier studies have addressed designs by simplifying the vapor flow path as a parallel plate duct (Steeves *et al.*, 2008). More in line with the structurally efficient designs discussed here, the vapor pressure drop will

be influenced by the chosen core topology, as differing topologies impart characteristic frictional losses on the vapor flow.

Chi (1976) has shown that the vapor pressure gradient along a heat pipe is given by;

$$\frac{dP_v}{dx} = -F_v q - D_v \frac{dq^2}{dx} \quad (3)$$

where x is the axial position, F_v and D_v are the frictional and dynamic coefficients for the vapor flow, respectively, and q is the local axial heat transfer rate. The frictional coefficient for the vapor flow is given by;

$$F_v = \frac{(f Re) \mu_v U}{2A_v^2 H \rho_v \lambda} \quad (4)$$

where f is the drag coefficient, Re is the Reynolds number, μ_v is the vapor dynamic viscosity, U is the vapor space perimeter, H is the vapor space height, A_v is the vapor space area, ρ_v is the vapor density, and λ is the latent heat of vaporization (Chi, 1976). Because q is zero at both ends of the heat plate, the second term on the right hand side of equation (3) drops out on integrating. Substituting equation (4) into (3) and integrating over the length of the heat plate (in the direction opposite vapor flow) provides an expression for the total vapor pressure drop;

$$\Delta P_v = \frac{(f Re) \mu_v UL}{2A_v^2 H \rho_v \lambda} q \quad (5)$$

where the Reynolds number can be expressed as a function of the heat transfer rate;

$$Re = \frac{H}{\lambda \mu_v A_v} q \quad (6)$$

From expression (5), it is clear that the total pressure drop is linearly dependent on the product of the friction factor and Reynolds number. In order to minimize the vapor pressure losses and push the capillary limit upwards, it is ideal to select a core topology which has a low friction factor at a given Reynolds number, which can be determined from expression (6) when the input heat flux is known. Expression (5) is valid for vapor space geometries in which pressure losses are due mainly to viscous drag, such as circular, rectangular, or corrugated ducts. For lattice frame, Kagome, and woven wire screen materials, where form drag dominates viscous drag, numerical and experimental methods have been used to determine ΔP_v (Tian *et al.*, 2004, Kim *et al.*, 2004). Figure 4 shows various core topologies as they relate to f and Re . Corrugated ducts and louvered fin geometries would be best,

while lattice frame materials (LFM's) and Kagome trusses would push the capillary limitation to lower values (thereby lowering the ultimate heat transfer limit) which may adversely affect performance. It should be noted, however, that structural performance and other thermal transport factors may dictate which core topology is optimal.

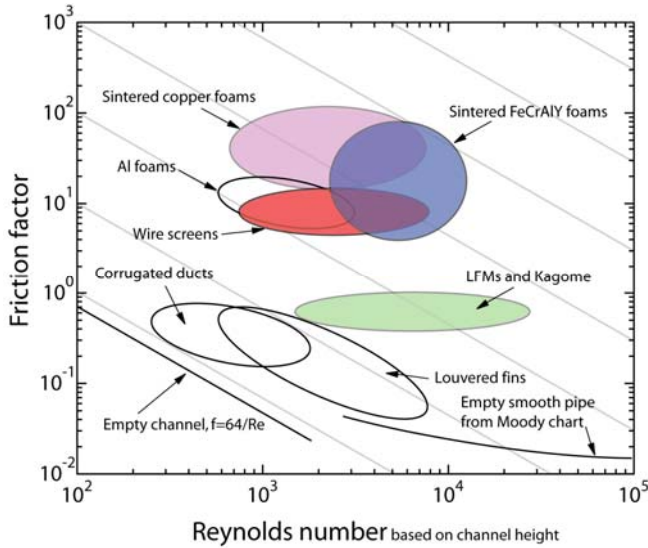


Figure 4. Friction factors of various core topologies as a function of the Reynolds number. The lightened diagonal lines indicate contours of constant ($f Re$). Adapted from Tian *et al.* (2004).

FABRICATION AND TESTING

Prototype fabrication and experimental setup. To demonstrate the heat spreading effectiveness of the leading edge concept and its potential for the hypersonic thermal environment, a low-temperature copper system using a water working fluid was designed, fabricated and tested. A truncated honeycomb core formed the vapor space, and all interior surfaces were lined with four layers of a sintered 100x100 copper mesh to serve as the wick. A photograph showing a cross-sectional interior view of the heat plate is shown in Figure 5. Two test articles were fabricated. A first was evacuated to 10^{-6} Torr and charged with distilled water sufficient to completely saturate the wick at room temperature. The second was evacuated to the same base pressure but was not charged with the working fluid.

The beam from a 2kW (maximum) Nd:YAG laser was scanned along the leading edge tip to create a localized heat flux estimated to be 78kW/m^2 . All external surfaces were allowed to cool by free convection and radiation. An infrared thermal imaging camera was used to capture temperature data over the top surface of the test article. More extensive details of the fabrication and experimental setup can be found in Kasen *et al.* (2008).

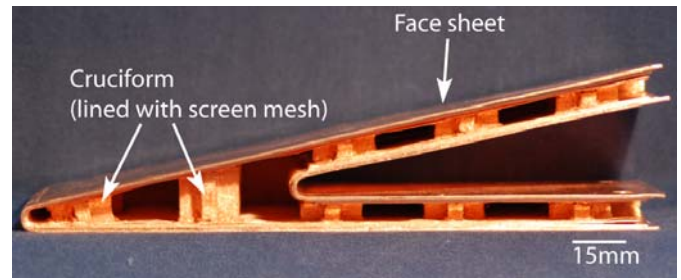


Figure 5. Photograph of a cross-sectional view of the truncated honeycomb leading edge heat plate before the side face sheets were installed.

Results and discussion. Figure 6 compares the axial temperature profile of the water-charged and evacuated heat plates after 5 minutes. The functioning heat plate shows a sharp temperature drop (approximately 12°C) up to a normalized position of 0.10 (from the heat source) of the axial length. The temperature profile from a position of 0.10 (beginning of the condenser zone) to 0.60 remains nearly isothermal. The temperature over the remaining portion of the condenser zone gradually decreases, which others have suggested is indicative of the presence of non-condensable gases in the system (Chi, 1976). The maximum temperature at 5 minutes is reduced by approximately 30% in the copper-water heat plate, and the overall thermal gradient is reduced by over 60%.

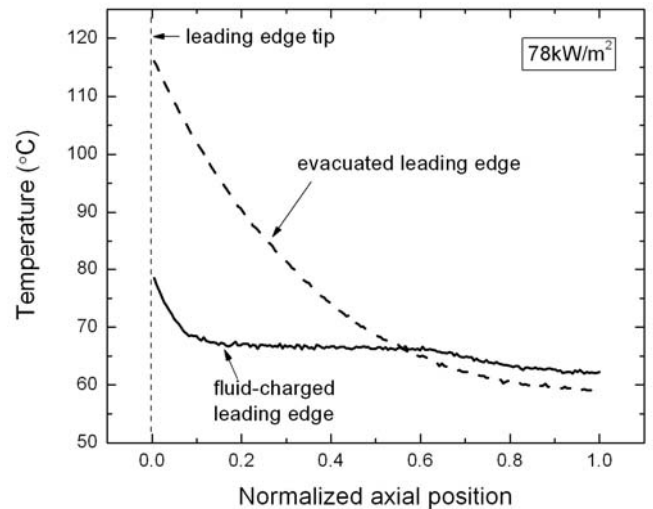


Figure 6. Temperature profile showing the axial temperature distribution on the top, outer face sheet of the copper leading edge absent a working fluid (evacuated) and the copper-water leading edge heat plate (fluid-charged), subjected to a 78kW/m^2 heat flux at its tip (at a normalized position of 0.0) for 5 minutes.

This profile trend is in good agreement with the work of Steeves *et al.* (2008), whose finite element models showed a similar axial temperature profile for a high temperature Inconel-Na and Cb752-Li leading edge heat pipe. The temperature drop near the stagnation tip is consistent with thermal conduction effects along the face sheets, corroborated by an identical thermal gradient in the evacuated heat plate over that length, which is transferring heat axially by thermal conduction only. From a design perspective, it is imperative that the choice of material at the leading edge tip be capable of sustaining the thermal stresses imposed on that region.

A plot of the leading edge tip temperature, which is also the maximum temperature, as a function of time is shown in Figure 7. Throughout the entire recorded period, the maximum temperature of the fluid-charged system is cooler than that of the evacuated system. After a short transient period ($t=30$ s), the tip temperature of the functioning system is approximately 15°C degrees cooler, an indication that the heat plate is already functioning. It should be expected that thicker face sheets than those used here (1.57 mm) would delay startup since the length of the thermal conduction pathway from the outer surface to the saturated wick / vapor interface would then be increased.

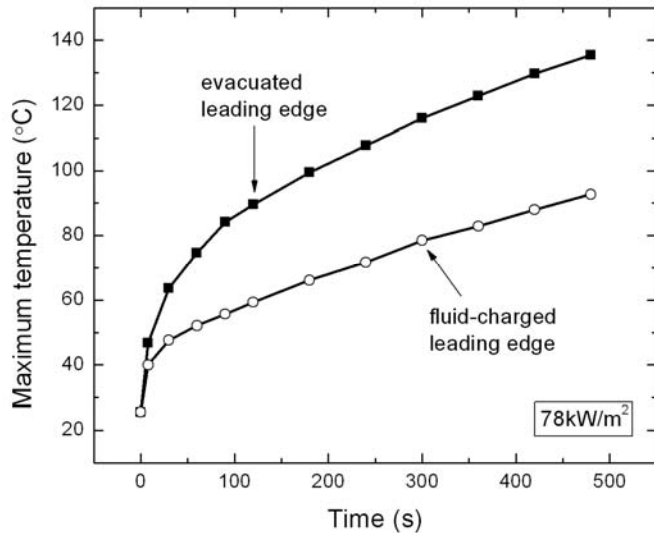


Figure 7. The maximum temperature as a function of time for the fluid-charged and evacuated leading edges.

Lumped thermal capacitance model. If the Biot modulus is low (<0.1), a simple lumped thermal capacitance model can be used to analyze the leading edge response. The Biot modulus indicates that the internal thermal conduction resistance is negligible in comparison with surface convection resistance (Holman, 1976). As noted elsewhere (see Faghri, 1995, Faghri and Harley, 1994), this requirement suits heat pipes well since their operation achieves a nearly homogenous temperature distribution (assuming thin container walls and wick structure).

An energy balance for the heat plate can be expressed as;

$$\Pi \frac{dT(t)}{dt} = q - hS(T(t) - T_f) \quad (7)$$

where Π is the total heat capacitance, $T(t)$ is the homogenous temperature at time t , q is the total power input, h is the heat transfer coefficient for convective cooling, S is the external surface area exposed to the ambient, and T_f is the surrounding (ambient) fluid temperature. Due to the small vapor mass, the vapor heat capacity is considered negligible. Then, the total heat capacitance can be expressed as

$$\Pi = (1 - \varphi)\rho_s V_w c_s + \varphi \rho_l V_w c_l + \rho_s V_s c_s \quad (8)$$

where φ is the wick porosity, V_w and V_s are the wick and solid copper volumes, ρ_l and ρ_s are the liquid water and solid copper densities, and c_l and c_s are the liquid water and solid copper specific heat capacities. Values for the variables are presented in Table 2. Integration of equation (7) requires an initial condition. Assuming the heat plate is in thermal equilibrium with the surrounding environment at $t=0$, the initial condition becomes $T(0) = T_f$. Integration of equation (7) provides an expression for the transient temperature response of the heat plate:

$$T(t) = T_f + \frac{q}{hS} (1 - e^{-t/\tau}) \quad (9)$$

where the time constant is $\tau = \Pi / hS$.

Variable	Value
φ	0.35
V_w	$3.39 \times 10^{-5} \text{ m}^3$
V_s	$7.72 \times 10^{-5} \text{ m}^3$
S	0.0489 m^2
ρ_s	8960 kg/m^3
ρ_l	998 kg/m^3
c_s	385 J/kgK
c_l	4181 J/kgK

Table 2. Relevant design variable and material property values.

A comparison of this model to the experimental temperature data of the copper-water heat plate is shown in Figure 8(a) with $T_f = 25^\circ\text{C}$, $h = 5 \text{ W/m}^2\text{K}$, and $q = 50 \text{ W}$. The values for h and q were established by comparing the transient temperature profiles of a solid copper wedge, tested under identical conditions, to a finite difference model. Details

can be found in Kasen *et al.* (2008). In order to remove the conduction effects near the leading edge tip, which are not accounted for in this model, the experimental values shown in the figure are average temperatures taken over a normalized position of 0.1 to 1.0. The model tends to underpredict the heat plate temperature over the entire transient period. A measure of the temperature deviation from the experimental results is calculated as

$$\delta(t) = \frac{T_e(t) - T_m(t)}{T_e(t)} \quad (10)$$

where the subscripts *e* and *m* refer to the experimental and model values. The deviation, plotted in Figure 8(b), shows the model underpredicts the observed values by a maximum of about 15%, with the rate of deviation largest in the early transient period. It is hypothesized that the input power may be slightly underestimated, contributing to the underprediction of the model temperature values (Kasen *et al.*, 2008).

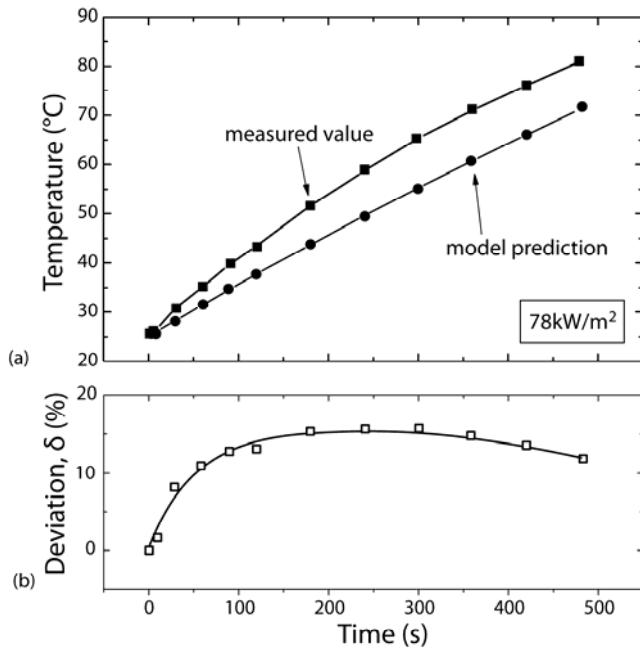


Figure 8. Comparison of the model with the measured values (a) and their deviation (b) as a function of time.

SUMMARY

A novel leading edge structural heat plate concept has been presented for effective thermal spreading of the stagnation point heat flux. A low-temperature, copper-water leading edge heat plate having a truncated honeycomb core has been designed, fabricated, and tested. Axial temperature profiles demonstrate effective thermal spreading, an indication that the concept shows promise for much higher heat fluxes and temperatures found during hypersonic flight.

ACKNOWLEDGEMENTS

Funding has been provided by the Office of Naval Research through the MURI program Revolutionary Materials for Hypersonic Flight (Contract No. N00014-05-1-0439) and by NASA through the Virginia Space Grant Consortium.

REFERENCES

S W Chi. *Heat Pipe Theory and Practice*. Hemisphere Publishing, Washington DC, 1976.

A G Evans, J W Hutchinson, M F Ashby. Cellular metals. *Current Opinion in Solid State and Materials Science*, 2:288-303, June 1998.

A G Evans, J W Hutchinson, N A Fleck, M F Ashby, H N G Wadley. The topological design of multifunctional cellular metals. *Progress in Materials Science*, 46:309-327, 2001.

A Faghri. *Heat Pipe Science and Technology*. Taylor & Francis, New York, 1995.

A Faghri and C Harley. Transient lumped heat pipe analysis. *Heat Recovery Systems & CHP*, 14(4): 351-363, 1994.

J A Fay and F R Riddell. Theory of stagnation point heat transfer in dissociated air. *Journal of the Aeronautical Science*, 25(2):73-85, February 1958.

J P Holman. *Heat Transfer*. McGraw-Hill, New York, 1973.

D A Kourtides. Thermal performance of composite flexible blanket insulations for hypersonic aerospace vehicles. *Composites Engineering*. 3:805-813, 1993.

J Lim and K Kang. Mechanical behavior of sandwich panels with tetrahedral and Kagome truss cores fabricated from wires. *International Journal of Solids and Structures*. 43(17):5228-5246, August 2006.

S Kasen, D T Queheillalt, C A Steeves, A G Evans, and H N G Wadley. Thermal performance of a heat plate leading edge. *In preparation*, 2008.

T Kim, H P Hodson, and T J Lu. Fluid-flow and endwall heat-transfer characteristics of an ultralight lattice-frame material. *International Journal of Heat and Mass Transfer*, 47(6-7):1129-1140, 2004.

J H Lundell. Spallation of the Galileo probe heat shield. In *Progress in Astronautics and Aeronautics*. P E Bauer and H E Collicott, eds., AIAA, Reston Virginia, 85:419-445, 1983.

D B Paul, C L Clay, B Harber, H Croop, D Glass, S Scotti. Extreme environment structures. In *Progress in Astronautics and Aeronautics*. A K Noor, ed., AIAA, Reston Virginia, 188:145-197, 2000.

D T Queheillalt and H N G Wadley. Pyramidal lattice truss structures with hollow trusses. *Materials Science and Engineering A*. 397(1-2):132-137, April 2005.

R Savino, M D Fumo, L Silverstroni, D Sciti. Arc-jet testing on HfB₂ and HfC-based ultra high temperature ceramic materials. *Journal of European Ceramic Society*. In press. 2008.

C A Steeves, M Y He, S D Kasen, L Valdevit, H N G Wadley, and A G Evans. Feasibility of Metallic Structural Heat Pipes as Sharp Leading Edges for Hypersonic Vehicles. *Journal of Applied Mechanics*, In press. 2008.

J Tian, T Kim, T J Lu, H P Hodson, D T Queheillalt, D J Sypeck, and H N G Wadley. The effects of topology upon fluid-flow and heat transfer within cellular copper structures. *International Journal of Heat and Mass Transfer*. 47(14-16):3171-3186, July 2004.

H N G Wadley. Multifunctional periodic cellular metals. *Philosophical Transactions of the Royal Society A*. 364:31-68, 2006.

H N G Wadley, N A Fleck, and A G Evans. Fabrication and structural performance of periodic cellular metal sandwich structures. *Composites Science and Technology*. 63(16):2331-2343, December 2003.

Z Wei, K P Dharmasena, H N G Wadley, A G Evans. Analysis and interpretation of a test for characterizing the response of sandwich panels to water blast. *International Journal of Impact Engineering*. 34(10):1602-1618, October 2007.

N Wicks and J W Hutchinson. Optimal truss plates. *International Journal of Solids and Structures*. 38(30-31):5165-5183, July 2001.

